Data Fusion of GEO *FY-4A* GIIRS and LEO Hyperspectral Infrared Sounders with Surface Observations: A Hong Kong Case Study

JESSICA MAIER[a,b] AND ROBERT KNUTESON[a,b]

[a] *Cooperative Institute for Meteorological Satellite Studies, Madison, Wisconsin*
[b] *Space Science and Engineering Center, University of Wisconsin–Madison, Madison, Wisconsin*

(Manuscript received 17 June 2021, in final form 15 October 2021)

ABSTRACT: Hyperspectral infrared satellite observations from geostationary platforms allow for the retrieval of temperature and water vapor measurements with higher temporal and vertical resolution than was previously available. The Chinese satellite *Fengyun-4A* (*FY-4A*) includes the Geostationary Interferometric Infrared Sounder (GIIRS), which has the ability to measure vertical profiles of temperature and water vapor from space at times when ground-based upper-air soundings are not available and can fill an important need in short-range weather prediction. In this study, convective available potential energy (CAPE) and lifted index (LI), which are used for forecasting atmospheric instability, were computed using the SHARPpy algorithm used by the NWS Storm Prediction Center. However, remote infrared and microwave sensing is lacking detailed information in the boundary layer, so the addition of the NOAA Meteorological Assimilation and Data Ingest System (MADIS) surface data may be necessary in order to get accurate temperature and moisture measurement near the surface. This study uses 10–16 May 2019 in the coastal region near Hong Kong for evaluating the use of hourly surface observations combined with satellite soundings from *FY-4A* GIIRS at 2-h intervals. The GIIRS plus MADIS surface-based CAPE and LI estimates are compared to estimates derived from low-Earth-orbiting (LEO) *SNPP* and *NOAA-20* from NOAA, MetOp from EUMETSAT, NWP reanalysis, and local radiosondes. In the case study, the 2-h sampling interval of the GIIRS geostationary sounder was able to capture the rapid transition (16 h) from a stable to an unstable atmosphere in both CAPE and LI. The use of surface observations with satellite soundings gave mixed results, possibly due to the complex terrain near Hong Kong.

KEYWORDS: Atmosphere; Asia; Coastal meteorology; Radiosonde/rawinsonde observations; Remote sensing; Satellite observations; Soundings

1. Introduction

The history of satellite sounding of Earth's atmospheric temperature and water vapor vertical profiles began with infrared and microwave sensors with relatively low spatial (~50 km) and vertical resolution (~2–3 km) (Smith 1991; Schmetz and Menzel 2015; Menzel et al. 2018). The High-resolution Interferometer Sounder (HIS) program at the University of Wisconsin–Madison Space Science and Engineering Center (SSEC) and the Cooperative Institute for Meteorological Satellite Studies (CIMSS) was started in the 1980s as an airborne demonstration of the value of hyperspectral infrared radiance observations to achieve higher vertical resolution (~1 km) at higher spatial resolution (~2 km) (Smith et al. 1987). Subsequently, the NASA Atmospheric Infrared Sounder (AIRS) was launched on the *Aqua* satellite in 2002, followed by the MetOp series of satellites with the Infrared Atmospheric Sounding Interferometer (IASI) in 2006 (and 2012 and 2018) (Chahine et al. 2006; August et al. 2012). The Cross-track Infrared Sounder (CrIS) joined the satellite constellation with NASA's *Suomi NPP* satellite in 2011 and most recently on the *NOAA-20* operational satellite in 2018. All these polar-orbiting satellites are significantly contributing to the global data assimilation that numerical weather prediction centers use for medium-range forecasting (Joo et al. 2013). However, the original goal of the HIS program was to combine the vertical resolving power of accurate high-spectral-resolution infrared measurements with the higher temporal refresh and higher spatial resolution achievable from a geostationary platform (Smith et al. 2009). The first on-orbit demonstration of a geostationary hyperspectral IR sounder is the Geostationary Interferometric Infrared Sounder (GIIRS), which is on board the Chinese *Fengyun-4A* satellite launched in 2016 followed by an operational GIIRS on board *Fengyun-4B* launched in June 2021 (Yang et al. 2017). The Infrared Sounder (IRS) is planned for geostationary orbit on the Meteosat Third Generation (MTG-S) satellite with substantially higher spatial resolution and higher temporal coverage rates (Holmlund et al. 2021). The geostationary platform has the advantage of sampling the atmosphere over a region throughout the diurnal cycle due to the large number of observations that are ideal for understanding the evolution of atmospheric stability on regional scales (Schmit et al. 2009; Holmlund et al. 2021). In addition, a geostationary platform allows for targeted observations and therefore more sensitivity for smaller changes in the regional atmospheric structure. For example, if there is a region of large model uncertainty or the possibility of high impact weather, the satellite allows a given spot to be viewed with the same instrument at the same view angle.

Although the number of daily high-spectral-resolution infrared soundings has greatly increased in the past 20 years, satellite-based passive infrared sounders are limited by a lack

Corresponding author: Jessica Maier jmaier5@wisc.edu

DOI: 10.1175/JTECH-D-21-0080.1

of information content in the boundary layer between the surface and the free troposphere (Smith et al. 2021). Gartzke et al. (2017) showed the potential for fusion of temperature and water vapor profiles derived from the hyperspectral IR sounders with observations of the near surface air temperature and dewpoint for the improved calculation of atmospheric stability parameters. Ma et al. (2021a) found that using surface air temperature and moisture observations, the low-level atmospheric soundings can be improved, especially the soundings below the height of 600 hPa. From these fused profiles, thermodynamic derived stability indices, e.g., CAPE and lifted index (LI), have been shown to have comparable accuracy to radiosondes, but with large spatial area coverage and the potential for complete diurnal coverage (Gartzke et al. 2017). This has been demonstrated in real time at UW-SSEC using direct broadcast observations from the *SNPP* and Joint Polar Satellite System (JPSS) satellites combined with dense surface observations over the CONUS region (Bloch et al. 2019). This paper will describe our assessment of the first geostationary infrared sounder in characterizing the rapid evolution of atmospheric stability with diurnal sampling at 2-h intervals. The results of this study are expected to be relevant to the future use of the GEO IR sounders, which will provide a higher temporal sampling for future geostationary platforms. The objective of this paper is to illustrate the value in the fusion of scientific data to inspire these methods in operational use.

a. Background

A hyperspectral infrared sounder, the GIIRS, is operating aboard the Chinese *Fengyun-4A* (*FY-4A*) satellite (Yang et al. 2017). The GIIRS has a spectral resolution in the thermal infrared, which matches the JPSS CrIS sensors on *SNPP* and *NOAA-20*. It is the first geostationary interferometer that provides nearly continuous soundings of temperature and humidity, which can be combined with surface measurements for a study of atmospheric stability. The temporal resolution of GIIRS allows for four-dimensional winds profiles from GIIRS to provide better dynamic information to help during near-real-time forecasting (Ma et al. 2021a). From our literature review, research on the temperature and humidity profiling from *FY-4A* GIIRS is lacking despite it being one of the newest instruments in orbit. The geostationary platform has the advantage of sampling the atmosphere over a region throughout the diurnal cycle. Timely information from atmospheric and humidity profiling is crucial for characterizing the thermal state of the atmosphere (Weisz et al. 2015). Ma et al. (2021b), at the first time, using 15-min GIIRS radiance observations with a novel method, derived atmospheric four-dimensional (4D) horizontal wind fields, they also found that both the temporal and spatial information contributes to the 4D wind fields, and higher temporal resolution provides better 4D wind fields than the lower temporal resolution. One limitation of the passive infrared sounders is a lack of information in the lower portion of the boundary layer under certain thermodynamic conditions (Wulfmeyer et al. 2015). Building on the Gartzke et al. (2017) study, this paper describes a fusion of profiles derived from the hyperspectral IR sounders with in situ observations of surface air temperature and dewpoint. In this study, comparisons are made between GIIRS-derived vertical profiles of temperature and humidity and local observational data from a coincident radiosonde launch site in Hong Kong, China.

This study analyses a multiday period covering 10–16 May 2019 in a region surrounding Hong Kong. Hong Kong was chosen because of its coastal location and because it falls within the *FY-4A* GIIRS regional coverage with 2-h repeat time. In addition, the case study covers three meteorologically distinct time periods; these phases will be described in section 1b. One operational Chinese Meteorological Administration (CMA) radiosonde launch site in the area was used as truth for comparisons with *MetOp-A*/*B* IASI, GFS, and *SNPP*/*NOAA-20* NOAA Unique Combined Atmospheric Processing System (NUCAPS) vertical temperature and moisture profiles. In addition, Meteorological Assimilation and Data Ingest System (MADIS) surface data were used for a time series comparison of surface temperature and dewpoint for study of the diurnal cycle aspects of the ocean and land. *FY-4A* Advanced Geostationary Radiation Imager's cloud-top pressure and cloud fraction was assessed for its contribution to the local understanding of the meteorology. A meteorological interpretation of the land ocean contrast using CAPE, total precipitable water (TPW), and wind direction was used to assess GIIRS spatial and temporal sampling. This study demonstrates that geostationary hyperspectral infrared sensors can provide valuable diurnal vertical soundings for meteorological analysis in coastal locations.

b. Data

Five different data types were used in this preliminary study including *FY-4A* GIIRS, *FY-4A* Advanced Geostationary Radiation Imager (AGRI), *FY-4A* Lightning Mapping Imager (LMI), World Meteorological Organization (WMO) radiosonde network, and the MADIS surface station network, NOAA NUCAPS and EUMETSAT IASI. Each data type provides different temporal, spatial, and measurement resolutions.

1) *FY-4A* GIIRS INFRARED SOUNDER

Satellite data from *FY-4A* GIIRS were the main data for analysis in this study. The *FY-4A* satellite is in geostationary orbit and is operated by the China Meteorological Administration and is the first four-dimensional observation of the atmosphere in geostationary orbit (Yang et al. 2017). *FY-4A* was launched in late 2016 and data became available in early 2018. A total of four instruments fly on *FY-4A* including LMI, AGRI, the Space Environment Package (SEP), and the GIIRS. Because *FY-4A* is equipped with GIIRS, it has the ability to sample vertical temperature and moisture, which is not available on any other geostationary satellite in the world.

GIIRS preliminary level 2 soundings were used in this study. GIIRS data were found at http://satellite.nsmc.org.cn using the file name FY4A-_GIIRS-_N_REGC_1047E_L2-_AVP-.nc and FY4A-_GIIRS-_N_DISK_1047E_L2-_AVP.nc-. Since *FY-4A* is geostationary, it always has the same field of view, but it does include two separate file domains; the full viewing disk and a regional domain covering China. The regional file contains hourly data for a region centered on China roughly 5000 × 5000 km^2. The disk file contains 3-hourly data. GIIRS has a spatial resolution of 16 km and can sample a specific location more than 20 times per day (Yang et al. 2017). However, some issues arise with temporal sample matching with other data because GIIRS does not collect observations around 1800 UTC. A number of observations are available within each file including atmospheric temperature, atmospheric humidity, surface temperature, pressure, surface pressure, various convective indices, ozone, latitude, and longitude. GIIRS processing uses 101 levels to define the atmosphere. These levels are the same as fixed AIRS L2 pressure levels. GIIRS data were selected using the given quality control product. The CMA has four quality control levels: 0 = perfect, 1 = good, 2 = bad, 3 = do not use. Quality control level 3 was not used in this study, only levels 0, 1, and 2. The quality control is based on cloud detection from AGRI Cloud products as well as an outlier elimination scheme using a biweight check.

2) *FY-4A* LIGHTING MAPPER IMAGER

The *FY-4A* satellite carries the LMI, which is able to provide continuous observations of total lightning (Hui et al. 2020). It was designed to identify early warnings of severe weather in China. For example, dense lightning is often associated with cumulus clouds and developing convection. These data can be used in conjunction with other geostationary observations to provide a complete picture of severe weather. The frequency and availability of LMI data will help forecasters identify regions of convection. Figure 1 shows an example of LMI energy and MODIS imagery on a day of intense convection in the Hong Kong region.

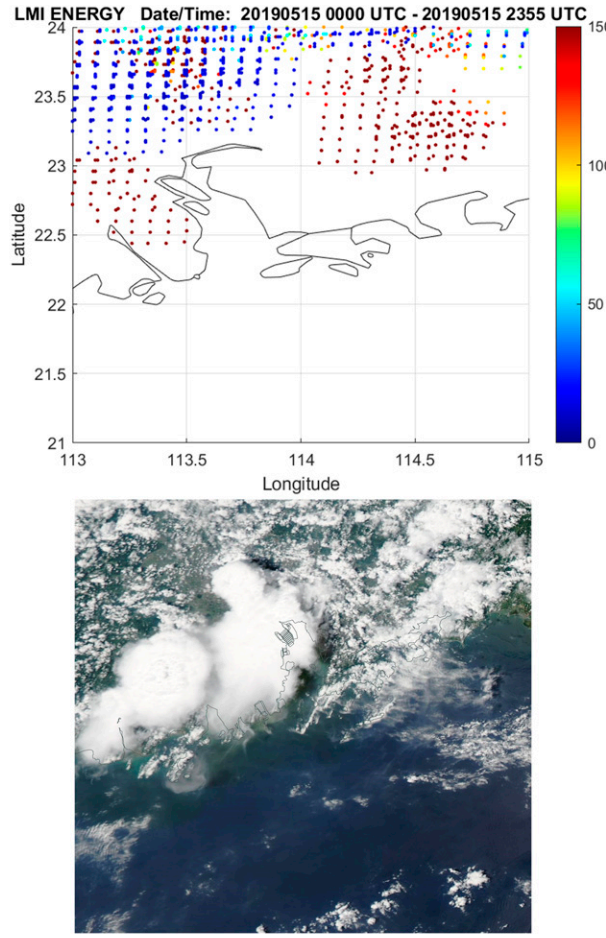

FIG. 1. (top) LMI total energy daily composite and (bottom) *Terra* MODIS true color imagery for 15 May 2019.

3) *FY-4A* AGRI

The *FY-4A* satellite carries AGRI, which is a 14-channel imager, similar to the GOES-R Advanced Baseline Imager (ABI) imager (Yang et al. 2017). Earth is sampled at 1 km at nadir in the visible, 2 km in the near-infrared, and 4 km in the remaining IR spectral bands. AGRI features a two-mirror structure, capable of flexible sensing in two dimensions, and minute-level fast sector scanning. Many products can be produced from AGRI including cloud masks, cloud type, cloud amount, rainfall rate, precipitable water, aerosol detection, cloud-top height, cloud-top pressure, cloud optical depth, cloud liquid water, cloud particle distribution, aerosol optical depth, convective initiation, and others (Min et al. 2017). These products can be found at https://satellite.nsmc.org.cn/PortalSite/Data/Satellite.aspx.

4) WMO RADIOSONDE NETWORK

The WMO provides a database with access to about 800 high-quality upper-air stations scattered throughout the globe (WMO 1996). These datasets are generally made two times a day at 0000 and 1200 UTC; however, some countries have slightly different release times and may only make observations once per day. These instruments record pressure, temperature, humidity, wind speed, and wind direction throughout the troposphere and stratosphere to about 30 km above the ground. They are run by individual countries meteorological services and the data are collected and made available through the Observing Systems Capability Analysis and Review Tool (OSCAR) at https://oscar.wmo.int/surface//index.html#/.

The CMA provides the WMO a network of radiosondes and OSCAR is a database that allows users to access this network of global observations. This network currently uses the GTS1 digital radiosonde (product ID: HQQTdaqi001) (Feng 2006). Ma et al. compared Vaisala RS80, Cryogenic Frostpoint Hygrometer (CFH), and GTS1 radiosondes and found that they have comparable biases (Ma et al. 2011). The average relative dry bias produced by the GFS1 sensor is 10% below 500 hPa, 30% above 500 hPa, and 55% above 310 hPa. For humidity, the GTS1 radiosonde does not respond to humidity changes in the upper troposphere, and sometimes even in the middle troposphere, which could cause data shifts. The daytime temperature bias is relatively consistent between the Vaisala RS80 and GTS1 but produces

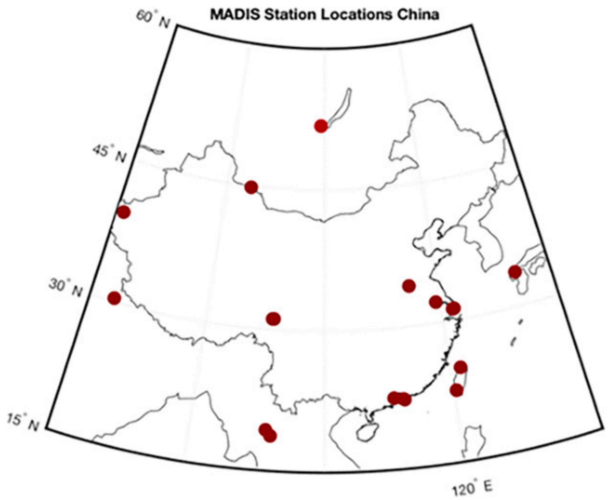

FIG. 2. The MADIS locations within China.

biases at night on the order of −0.2 to −1.6 K (Ma et al. 2011).

5) MADIS SURFACE STATIONS

The NOAA MADIS was used in this study because of its regular hourly measurements (Miller et al. 2005). MADIS provides hourly latitude, longitude, elevation, surface temperature, surface dewpoint, and surface pressure for a high density of stations throughout the world for account users. This system accumulates data in real time from participating countries throughout the world, including China. There are about 40 MADIS surface locations throughout the GIIRS domain and one within the Hong Kong region. Hourly surface observations files in netCDF format were found at https://madis-data.ncep.noaa.gov/public/sfcdump.html. The MADIS surface locations available within China are shown in Fig. 2. Quality control is preapplied to all MADIS observations during data processing.

6) NUCAPS

NUCAPS was developed to provide global atmospheric vertical temperature and moisture profiles from NOAA operational weather satellites, and has been extended to include EUMETSAT MetOp weather satellites (Gambacorta 2013). NUCAPS products are derived from the combined use of satellite-based microwave and infrared radiance observations. NUCAPS is currently used to process the CrIS and the Advanced Technology Microwave Sounder (ATMS) suite of instruments currently on board the NASA *SNPP* satellite and on *NOAA-20* as well as the IASI, the Advanced Microwave Sounding Unit (AMSU), and the Microwave Humidity Sounder (MHS) suite of instruments.

NUCAPS profile data were used in the study as representative LEO infrared soundings. This paper uses both NUCAPS soundings from the *SNPP* satellite and EUMETSAT MetOp weather satellites. The NUCAPS vertical profiles of temperature and water vapor mixing ratio are output on a fixed pressure scale with 100 vertical points (Gambacorta 2013). Data were retrieved from NOAA Comprehensive Large Array-data Stewardship System (CLASS) at https://www.avl.class.noaa.gov/saa/products/search?datatype_family=JPSS_SND.

7) IASI

IASI is the infrared sounder aboard the *MetOp-A* and *MetOp-B* satellites as part of the EUMETSAT Polar System (EPS) (August et al. 2012). Since 2006, IASI has provided information about Earth's infrared radiation emitted between 645- and 2760-cm^{-1} spectral range, an apodized spectral resolution of 0.5 cm^{-1} and radiometric noise of 0.2 K. Its sun-synchronous orbit is completed with an approximately 2100-km-wide swath and a total of 120 views along the swath. IASI is capable of measuring atmospheric composition as 24 atmospheric species have been identified. The product titled "IASI Atmospheric Temperature Water Vapor and Surface Skin Temperature–MetOp" for this study was retrieved from https://archive.eumetsat.int.

8) GFS

GFS was used as an example of a forecast model for purposes of consistent time intervals and spatial resolution. The GFS model is an operational NWP model that divides the globe and is divided into 1° × 1° grid points. GFS analysis data every 6 h were extracted at 22°N latitude and 114°E longitude. GFS data were extracted from ftp://ftp.ssec.wisc.edu/pub/eosdb/ancillary/, which is a component of the Community Satellite Processing Package (CSPP) (Gustiandi and Monica 2020). Temperature, moisture, pressure, surface measurements, and total precipitable water vapor were used in this study.

To estimate the model bias, we take advantage of the NCEP Global Data Assimilation System (GDAS), which optimally combines the 6-h forecast, or background, with the new observations, creating a new analysis. The analysis is the best estimate of truth we have after combining the model forecasts and the observations.

2. Methods

Since this study was conducted through a snapshot lens of a case study, details about specific local time are important for comprehension. For all figures in this study, units of time are in UTC, not local Hong Kong time. There is a conversion of +8 h to get from UTC to local time. For example, a 0000 UTC sounding would be released at 0800 local time and a 1200 UTC radiosonde at 2000 local time. This suggests there are no daytime radiosonde launches in Hong Kong, only early morning and late evening.

To calculate stability indices such as CAPE, CIN, and LI, vertical profiles of pressure, temperature, and water vapor were obtained for the time period from 10 to 16 May 2020 for a region centered on 22.32°N, 114.17°E, the location of the radiosonde launch site closest to Hong Kong. The Hong Kong region is defined as a box with coordinates ranging from 21° to 24°N latitude and from 113° to 115°E longitude, which is roughly 300 × 200 km^2. The locations of each sounding in relation to Hong Kong and the southern Chinese

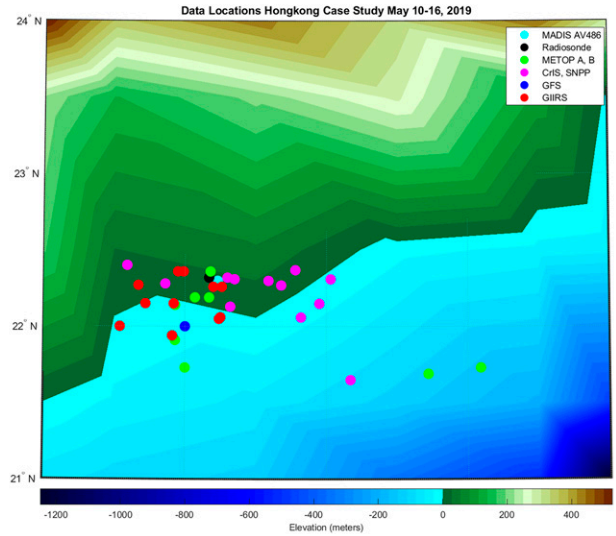

FIG. 3. The locations of the selected MADIS, radiosonde, IASI, NUCAPS, and GFS soundings from 10 to 16 May 2020 between 21° and 24°N latitude and between 114° and 119°W longitude.

coastline are shown in Fig. 3. The southern coast of China bordering the South China Sea is characteristic of coastal meteorology and has similar weather patterns to the southern U.S. Gulf of Mexico coastline.

Although each data type uses a different algorithm, this study uses a consistent analysis across all datasets. Values of CAPE were computed for each vertical profile using SHARPpy, described in Blumberg et al. (2017). SHARPpy is a Python software library that the research community can use and is derived from the Storm Prediction Center. Vertical soundings from IASI, GFS, and NUCAPS were selected by choosing the closest overpass location to the radiosonde launch site. Most of these satellite soundings are within 150 km as seen in Fig. 4. However, GIIRS data were subset to within 50 km of the radiosonde launch site. Those data were used in a calculation of the most amount of valid vertical data that pass the GIIRS predetermined quality control levels of 0, 1, or 2 as defined in section 1b. Figure 5 shows two methods for showing the amount of vertical data in each selected profile for the case study. A vertically averaged quality control variable was calculated for both the temperature and the humidity profiles as well as a summation of the amount of missing data in the vertical.

AGRI products like cloud fraction, clear fraction and cloud-top pressure were calculated by first applying quality control and then extracting the data contained in a box surrounding Hong Kong (21°–24°N, 112°–116°E). Cloud-top pressure was calculated by averaging the extracted data. Clear and cloud fraction were also extracted for the region. The original AGRI product provides a cloudiness rating from zero to three. Zero is cloudy, one is probably cloud, two is probably clear, and three is clear. For this study, cloud fraction is the summation of all the zero and one categories divided by the total number of data for the box. Clear fraction is the total number of twos and threes divided by the total number of data for the box.

This paper utilizes the surface parcel method for calculating CAPE and CIN as outlined below:

$$\mathrm{CAPE} = g\int_{\mathrm{EL}}^{\mathrm{LFC}} \frac{(T_{v,\mathrm{parcel}} - T_{v,\mathrm{env}})}{T_{v,\mathrm{env}}}\,dz,$$

$$\mathrm{CIN} = g\int_{\mathrm{Psurf}}^{\mathrm{LFC}} \frac{(T_{v,\mathrm{parcel}} - T_{v,\mathrm{env}})}{T_{v,\mathrm{env}}}\,dz,$$

$$\mathrm{LI} = T_{e\ 500} - T_{p\ 500}.$$

3. Results

a. *Thermodynamic vertical profile analysis*

Figure 6 includes two vertical sounding comparisons between NUCAPS, IASI, GFS, GIIRS, and local radiosondes from 0000 UTC 10 May to 1200 UTC 14 May 2019. In

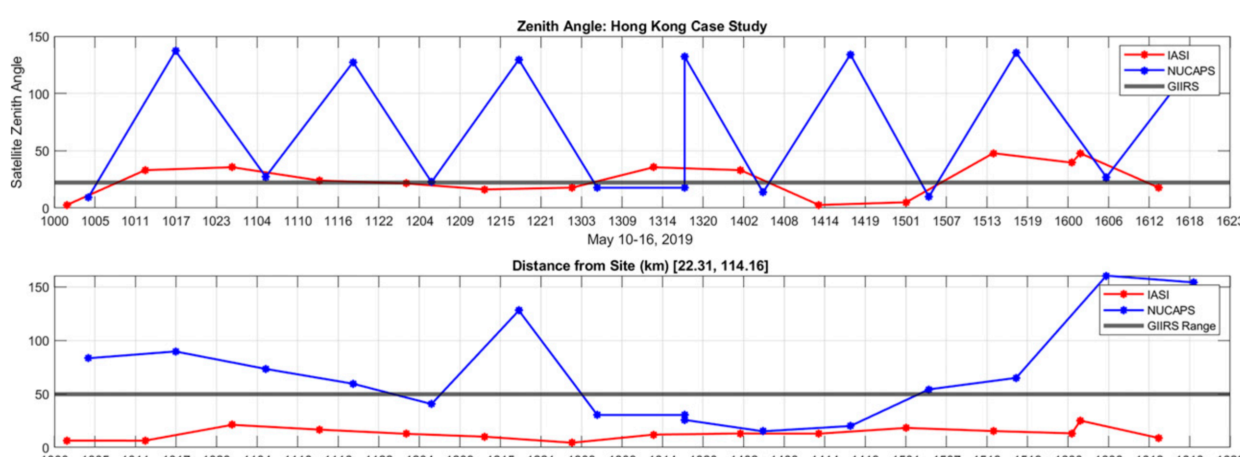

FIG. 4. NUCAPS and IASI (top) zenith angle and (bottom) distance from Hong Kong radiosonde launch site (22.31°N, 114.16°E).

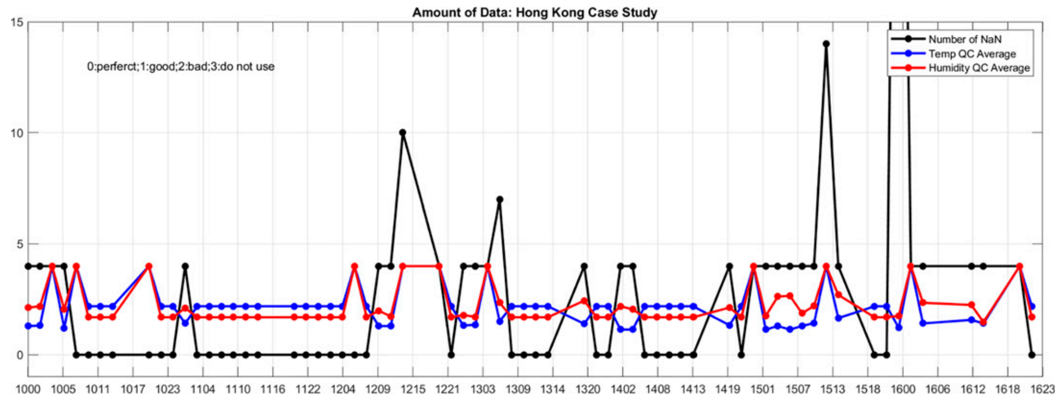

FIG. 5. Two methods for showing the quality and quantity of each GIIRS profile are shown. First a vertical average of the GIIRS quality control variable for both temperature (red) and humidity (blue). Second is a summation of the amount of missing data within the profile (black).

addition, vertical wind speed and direction are included from the WMO Hong Kong radiosonde. MADIS surface temperature and dewpoint are overlaid as symbols at the surface pressure for visualization of the differences between radiosonde and surface station temperature and dewpoint. The shaded regions visually represent the area of nonzero CAPE on the skew *T* diagrams. The stated CAPE, CIN, and LI are computed using the WMO Hong Kong radiosondes. These two time periods were chosen as characteristic dry (0000 UTC 10 May) and moist (1200 UTC 14 May) atmospheres in the region. (The transition to the moisture atmosphere is shown in Fig. 7.) GIIRS data do well in capturing the temperature profile; however, the humidity profiles for each time are degraded. Due to the application of GIIRS quality control, various parts of the GIIRS soundings are unusable and appear broken. In both cases, GIIRS is unable to observe the surface temperature and dewpoint.

b. *Diurnal atmospheric stability assessment*

To provide an estimate of cloudiness in the region, AGRI cloud-top pressure and GFS total precipitable water vapor were used in a time series. Figure 8 demonstrates that cloud-top pressure and TPW have an inverse relationship. The cloud-top pressure decreases and the TPW increases, which suggests clouds develop lower in the atmosphere while the column water vapor becomes moister.

MADIS surface data provide high-quality surface information every hour throughout the day. Therefore, comparisons can be made to satellite surface measurements with very little temporal error. Figure 9 shows GFS, IASI, NUCAPS, radiosonde, and MADIS surface temperature and dewpoint for the duration of the case study. Although temperature varies about by 6 K diurnally, daytime temperature in Hong Kong goes from 298 K on 10 May to 304 K on 16 May and dewpoint begins around 296 K and ends around 300 K. There is a sharp increase in both temperature and dewpoint at 2200 UTC 13 May.

Conversely to Fig. 9, Fig. 10 demonstrates the addition of the MADIS surface temperature and dewpoint and the effect it has on CAPE values. The colored circles represent the CAPE values without the addition of MADIS surface temperature and dewpoint. Each colored circle corresponds to a colored star, which represents the fused MADIS CAPE product. Near the second part of the case study, MADIS fused GFS, IASI, and NUCAPS CAPE greatly exceed the nonfused product.

4. Discussion

Satellite hyperspectral infrared soundings of temperature and moisture are useful in forecasting severe weather events, especially between operational radiosonde launches at 0000 and 1200 UTC as well as filling in observational spatial gaps. However, stability indices such as CAPE, CIN, and LI are often degraded near the surface due to inaccurate surface measurements from satellites. Gartzke et al. (2017) showed that in order to more accurately reflect the true surface parcel, spaceborne soundings should be combined with surface measurements of temperature and dewpoint. Bloch et al. (2019) showed that combining MADIS with NUCAPS CrIS retrievals greatly improved the underestimation of the surface temperature and humidity and therefore measurements of the corresponding stability indices.

a. FY-4A *AGRI and LMI*

As seen in Fig. 8, the column of precipitable water vapor increases dramatically during the duration of the case study due advection of moisture above the boundary layer. In addition, the atmosphere becomes increasingly unstable during this 6-day window. This is evident by AGRI clear and cloud fraction as well as lightning imagery, which is not included. These LMI lightning events indicate deep convection in the latter half of the case study. Cloud fractional coverage decreases throughout case study while cloud-top pressure increases and GFS TPW increases.

b. *NUCAPS*

Figure 10 shows some improvement of NUCAPS, IASI, and GFS soundings using MADIS surface measurements.

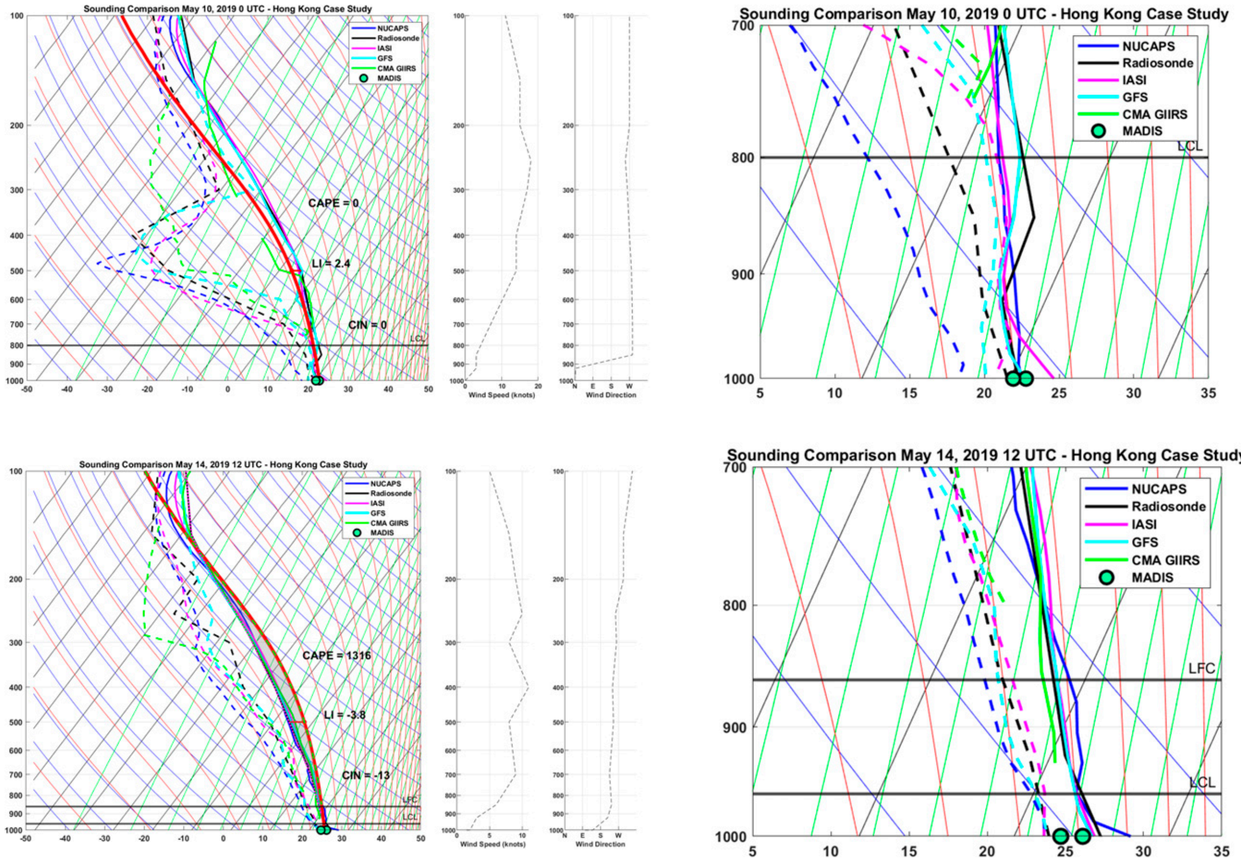

FIG. 6. Overlaid vertical profiles of temperature and dewpoint observed at (top) 0000 UTC 10 May and (bottom) 1200 UTC 14 May. Temperatures are represented by the solid lines and dewpoint lines are dashed. NUCAPS is shown in blue, local radiosondes in black, IASI in magenta, GFS in cyan, and GIIRS in green. Green and black circles are the MADIS surface temperature and dewpoint. (right) The local radiosonde wind speed and direction with respect to height. The red line represents the moist adiabat for the surface air parcel. (left) Just the boundary layer from 1000 to 700 hPa.

However, there are mixed results when comparing MADIS–NUCAPS fused CAPE and local radiosonde CAPE values. On 2200 UTC 13 May, the MADIS fused CAPE becomes closer to the local sounding CAPE values. However, in most cases after 0000 UTC 14 May, the addition of MADIS surface causes extreme overestimations of CAPE. This overestimation is thought to be because of complex coastal environment in Hong Kong location. NUCAPS +MADIS profiles on 14, 15, and 16 May have CAPE values over 5000 J kg^{-1}. These values are clear outliers and likely caused by NUCAPS having a 2°–3°C lower dewpoint than the local radiosonde.

c. IASI

As shown in Fig. 10, MADIS fused IASI shows a similar pattern to NUCAPS, in which, starting on 1200 UTC 13 May, a transition begins between typical coastal meteorology to a preconvective environment. When considering Fig. 9, it is clear that between 1200 UTC 13 May and 0000 UTC 14 May, a transition occurs from moisture mostly in the boundary layer to midtropospheric moisture. This developing midlevel moisture produced clouds at that level, which satellite-based infrared sounders have some difficulty identifying. These instruments' behavior varies in their retrieval in the presence of clouds. For example, the 0000 UTC 13 May IASI moisture profile is significantly drier at about 800 hPa, likely due to low-level cloud development. IASI is unable to detect these low-level clouds and diverges from the local radiosonde at this level.

d. GIIRS

Figure 9 shows wind speed and direction at the surface for the duration of the case study collected from MADIS samples. It is clear that thermal winds increase during daytime and decrease at night. The correlation between dewpoint and wind suggests moist air advection. The diurnal variation is likely explained by the land–ocean breeze, which is evident in AGRI imagery. Subsequently, variability in CAPE can be attributed to small-scale variations in coastal environments like onshore and offshore winds.

Over the duration of the case study, diurnal variation in wind speed is correlated with increases and decreases in

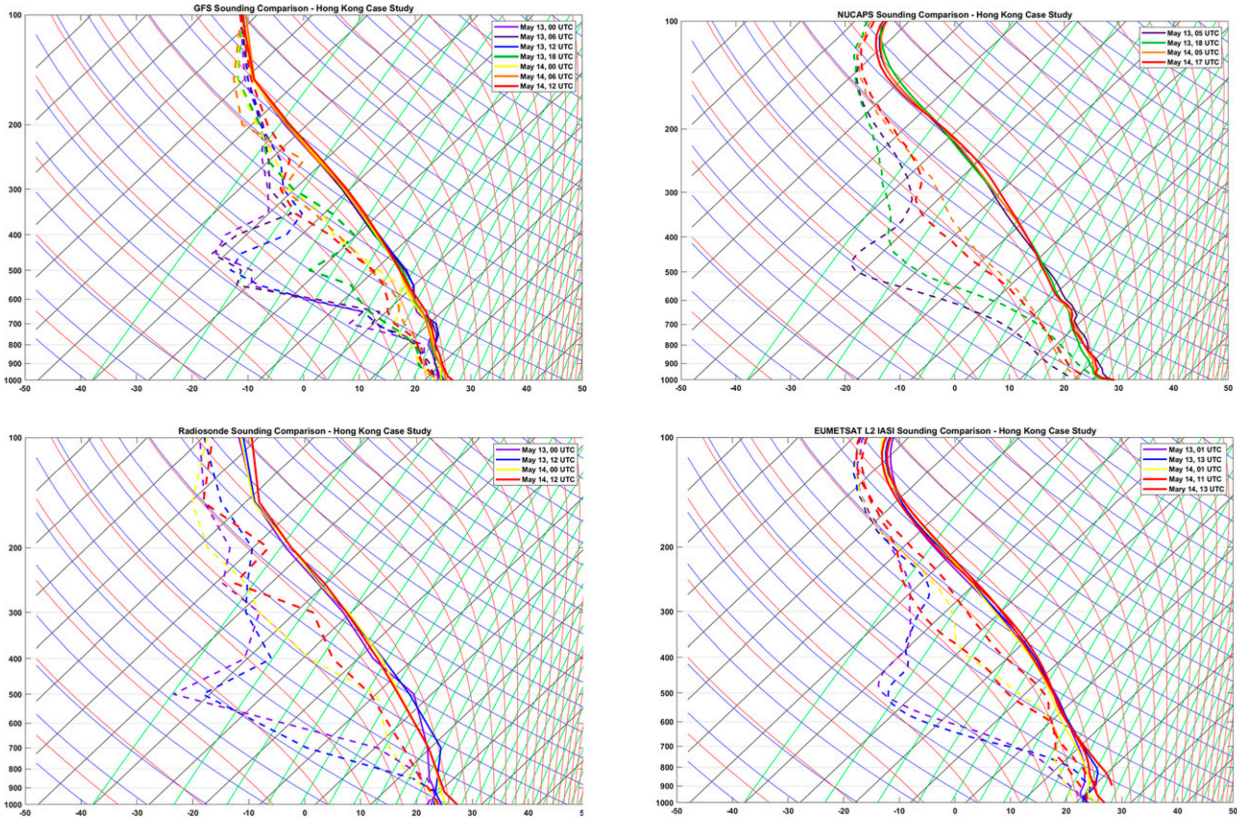

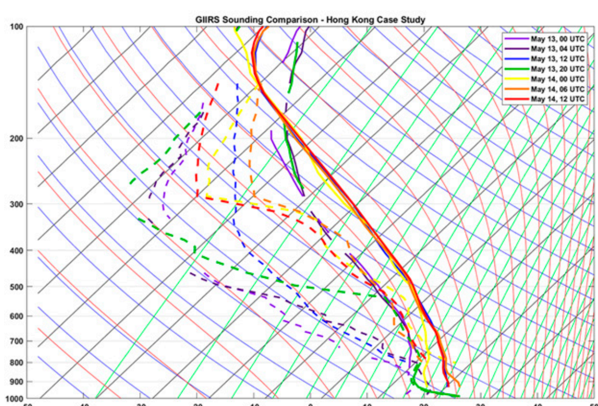

FIG. 7. Case study meteorological transition period from 0000 UTC 13 May to 1200 14 May for each of the datasets. (top left) The GFS data, (top right) the NUCAPS data, (middle left) the local radiosonde data, (middle right) EUMETSAT IASI data, and (bottom) GIIRS soundings.

temperature and dewpoint. Figure 9 shows a clear trend of increasing temperatures and dewpoints beginning 10 May, with coldest daytime temperature on 10 May and the highest daytime temperature occurring on 16 May. The case study can be roughly split into three phases characterized by the local meteorology; during 10–12 May, there are cooler temperatures and dewpoints and smaller CAPE values while 13–14 May is a clear transition period, and 15–16 May has a trend of CAPE greater than 1000 J kg^{-1} as well as being warmer and moister. When considering the transition period (see Fig. 12), the first phase tends to have lighter winds. During this period, the land and ocean breeze dominates due to diurnal advection by wind. Between 1200 UTC 13 May and 0000 UTC 14 May, also known as phase 2, a shift from generally dry to generally wet vertical profiles occurs. Along with this change, winds shift from northeast to southwest. While the first phase is mostly influenced by diurnal variations, phase 3 is dominated by strong southerly flow that brings moisture and convection, which is likely caused by advection of moisture from the ocean.

For phase 1 of the case study, the upper-level water vapor is relatively dry. However, on 14 May, the upper-level water vapor from 700 to 300 hPa increases due to advection from the South China Sea as seen in the GFS wind direction in Fig. 11. Figure 3 shows the Hong Kong coastline running from southwest to northeast, which is similar to the Gulf of

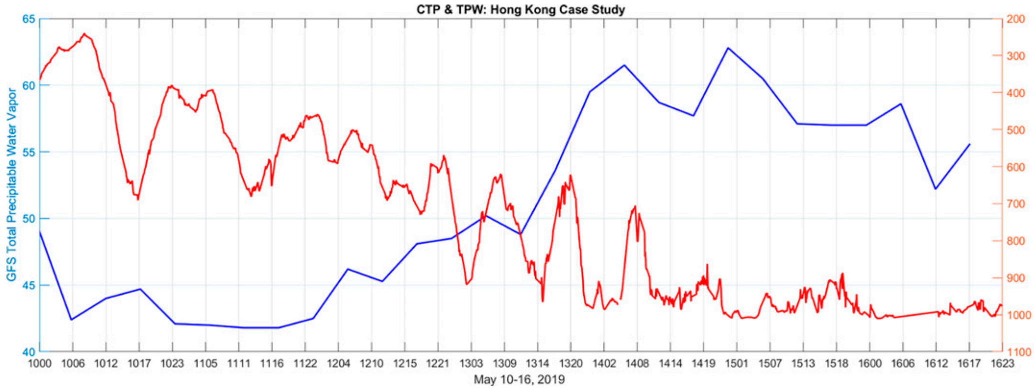

FIG. 8. AGRI cloud-top pressure (hPa; blue) reversed in the y direction to show the surface at the bottom and GFS total precipitable water vapor (mm; red) beginning 1000 UTC 10 May (1000) and ending 2300 UTC 16 May (1623).

Mexico geography. This suggests that warm moist air will generally originate over the ocean to the south and dry air from the north. This increase in upper-level moisture corresponds to an increase in CAPE and decrease of lifted index, also seen in Fig. 10. Another strategy for looking at the incoming moisture during the transition period is seen in Fig. 12 where both GFS model data and GIIRS show a warm moist air mass coming from the southwest. This transition is captured by the IR satellite soundings and verified by radiosondes in Fig. 7.

Other inconsistencies can be explained by temporal sampling differences up to 5 h. Since local radiosondes are released in the morning and the evening, it is difficult to validate CAPE outliers from IASI, NUCAPS, and GFS. The presence of GIIRS retrievals at 2-h intervals throughout the day will help to provide a better understanding of diurnal variation in CAPE.

5. Conclusions

Satellite estimates of the surface parcel introduce large uncertainties in CAPE estimates from inaccurate surface measurements (Gartzke et al. 2017). Satellite soundings struggle to provide accurate measurements in the lower-tropospheric region due to increased opacity of the atmosphere when viewed from space and in the presence of temperature inversions over land. However, in the case study, the 2-h sampling interval of the GIIRS geostationary sounder was able to capture the rapid transition (16 h)

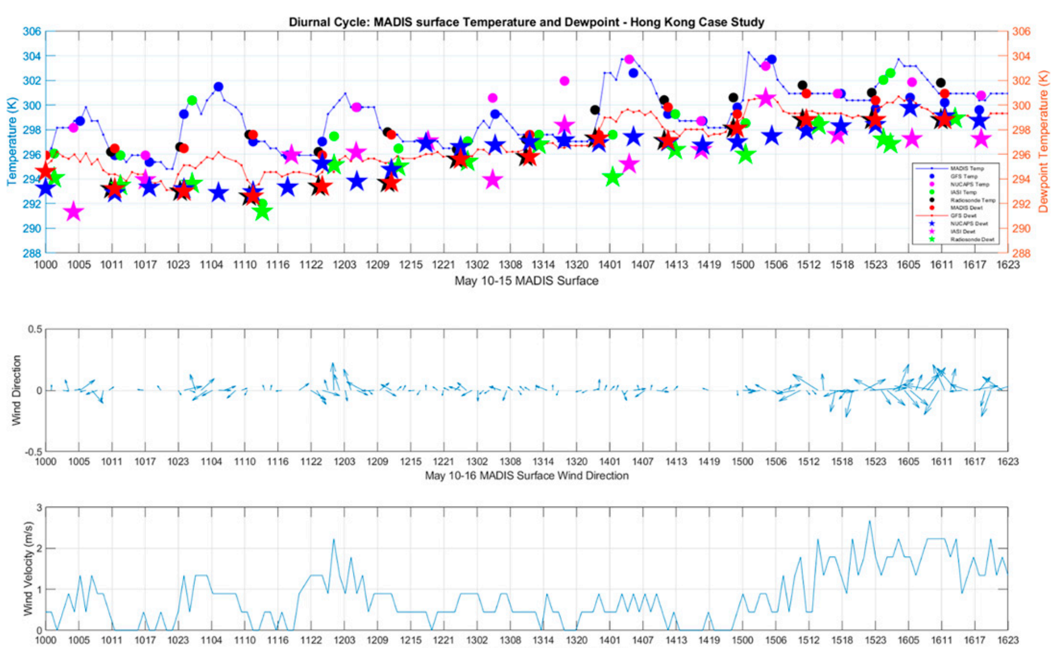

FIG. 9. The 10–16 May 2019 surface temperature and dewpoint from MADIS (blue and red lines), GFS (blue dots and stars), NUCAPS (magenta dots and stars), IASI (green dots and starts), (top) radiosonde (black dots and stars), (middle) MADIS surface wind direction, and (bottom) MADIS surface wind speed.

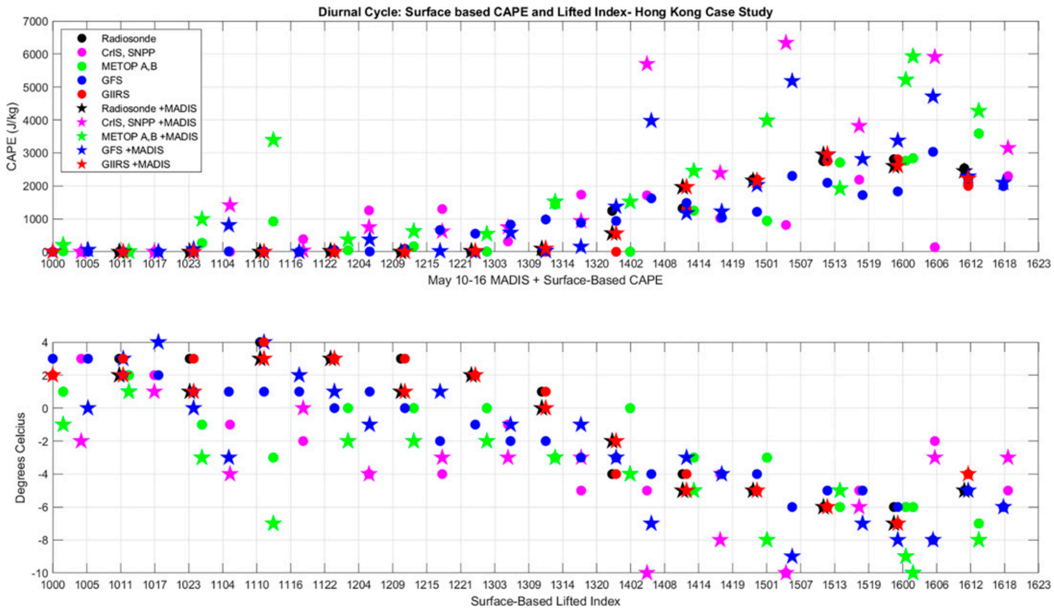

FIG. 10. The 10–16 May 2019 (top) CAPE and CAPE + MADIS and (bottom) LI and LI + MADIS from radiosondes, NUCAPS, IASI, and GFS.

from stable to unstable atmosphere in both CAPE and LI, which is consistent with the findings in a geostationary hyperspectral IR sounder simulation study (Li et al. 2011). In contrast, the polar-orbiting sounders provide sampling only at 12-h intervals. This highlights the advantage of a geostationary platform for sampling near-real-time weather.

This study produced mixed results in the fusion of satellite-based soundings and MADIS surface observations, likely due to moist air advection from coastal winds at the surface. Although

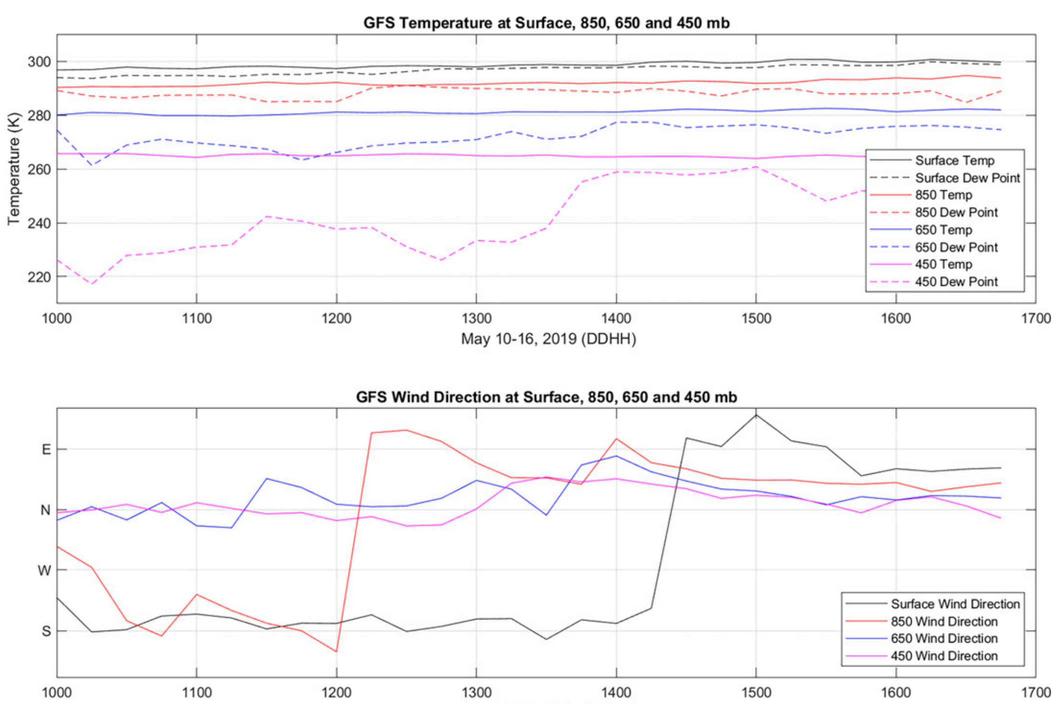

FIG. 11. (top) GFS temperature and dewpoint at the surface and 850, 650, and 450 hPa and (bottom) GFS wind direction at the same levels.

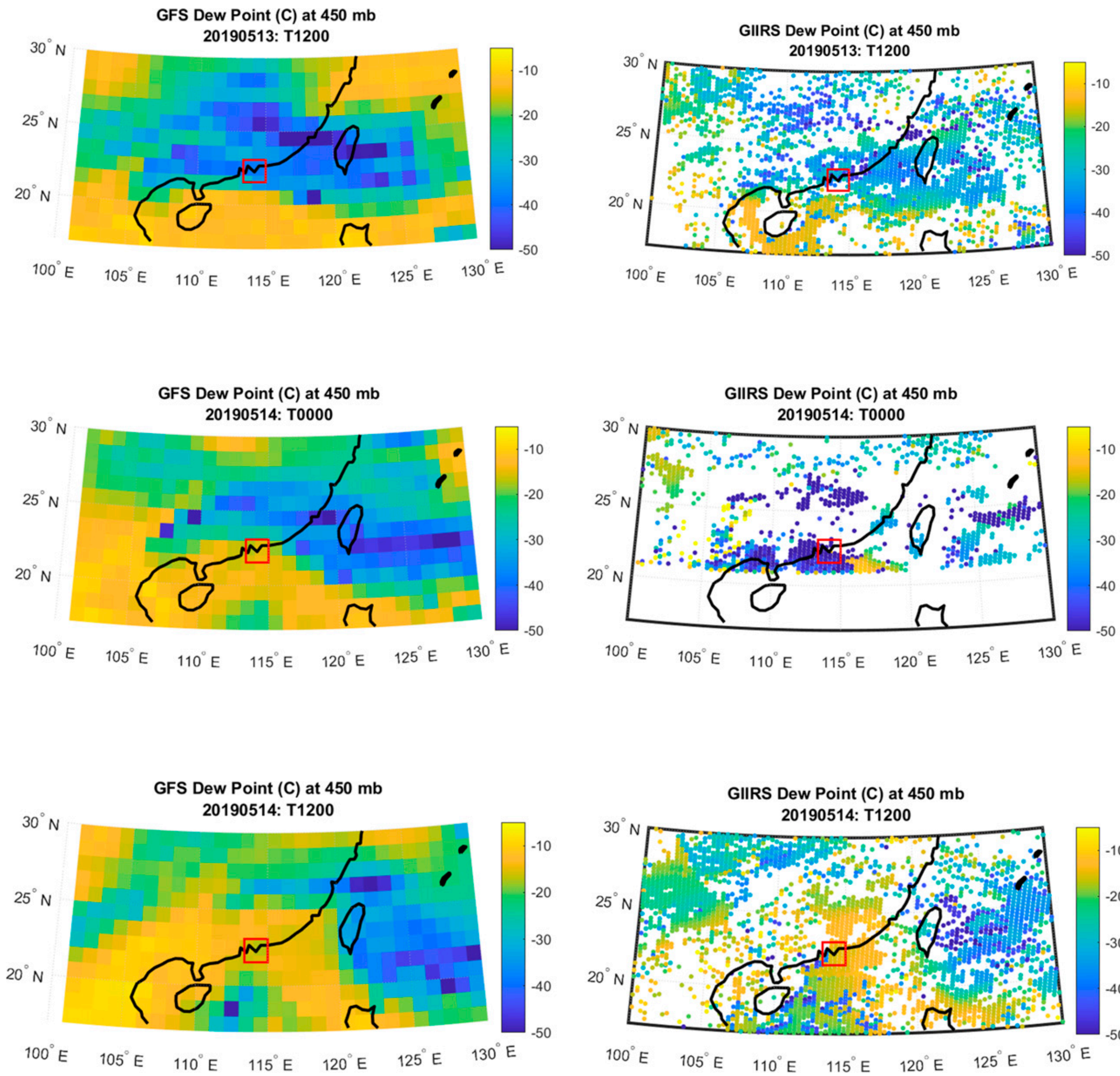

FIG. 12. (left) GFS and (right) GIIRS dewpoint temperature at 450 hPa for the transitional period at (top) 1200 UTC 13 May, (middle) 0000 UTC 14 May, and (bottom) 1200 UTC 14 May.

Gartzke et al. (2017) showed that the fusion of satellite and surface data improves the calculation of CAPE in the southern Great Plains, the presence of complex meteorology in coastal locations and the lack of surface observations can produce varied results. A more sophisticated approach, such as the consideration of local topography, for the fusion of these products may be needed for characterization of coastal environments. As discussed in section 4d, the merging of land-based surface observations with satellite soundings over the ocean requires careful consideration of the topography and local meteorology.

Future work will include an analysis of at least a year of GIIRS data. In addition, exploration of the use of GIIRS temperature and moisture profiles to assess diurnal change of coastal environments will be done in the context of NWP data assimilation.

This study is in support of a larger project to develop validation methods for the evaluation of GEO and LEO sounders to assess the ability of satellite passive sounders to monitor the diurnal characteristics of the planetary boundary layer. Our study provides important insights in atmospheric profiling from geostationary programs like *FY-4A* and instruments like GIIRS. The EUMETSAT Meteosat Third Generation (MTG) IRS sounder will provide geostationary information similar to GIIRS starting in about 2023. This analysis is anticipated to contribute to the NOAA GEO-XO studies for a future U.S. geostationary hyperspectral infrared sounder (Schmit et al. 2009).

Acknowledgments. This work was supported under NOAA Grant NA19OAR0220090. The authors thank Callyn Bloch for her assistance in reviewing and editing this manuscript.

REFERENCES

August, T., and Coauthors, 2012: IASI on MetOp-A: Operational level 2 retrievals after five years in orbit. *J. Quant. Spectrosc. Radiat. Transfer*, **113**, 1340–1371, https://doi.org/10.1016/j.jqsrt.2012.02.028.

Bloch, C., R. O. Knuteson, A. Gambacorta, N. R. Nalli, J. Gartzke, and L. Zhou, 2019: Near-real-time surface-based CAPE from merged hyperspectral IR satellite sounder and surface meteorological station data. *J. Appl. Meteor. Climatol.*, **58**, 1613–1632, https://doi.org/10.1175/JAMC-D-18-0155.1.

Blumberg, W. G., K. T. Halbert, T. A. Supinie, P. T. Marsh, R. L. Thompson, and J. A. Hart, 2017: SHARPpy: An open-source sounding analysis toolkit for the atmospheric sciences. *Bull. Amer. Meteor. Soc.*, **98**, 1625–1636, https://doi.org/10.1175/BAMS-D-15-00309.1.

Chahine, M. T., and Coauthors, 2006: AIRS: Improving weather forecasting and providing new data on greenhouse gases. *Bull. Amer. Meteor. Soc.*, **87**, 911–926, https://doi.org/10.1175/BAMS-87-7-911.

Feng, L., 2006: New development with upper air sounding in China. WMO Tech. Doc., 9 pp.

Gambacorta, A., 2013: The NOAA Unique CrIS/ATMS Processing System (NUCAPS). NOAA Algorithm Theoretical Basis Doc., 78 pp.

Gartzke, J., R. Knuteson, G. Przybyl, S. Ackerman, and H. Revercomb, 2017: Comparison of satellite-, model-, and radiosonde-derived convective available potential energy in the southern Great Plains region. *J. Appl. Meteor. Climatol.*, **56**, 1499–1513, https://doi.org/10.1175/JAMC-D-16-0267.1.

Gustiandi, B., and D. Monica, 2020: Current development of Community Satellite Processing Package (CSPP) to support direct broadcast remote sensing satellite data processing. *IOP Conf. Ser.: Earth Environ. Sci.*, **500**, 012016, https://doi.org/10.1088/1755-1315/500/1/012016.

Holmlund, K., and Coauthors, 2021: Meteosat Third Generation (MTG): Continuation and innovation of observations from geostationary orbit. *Bull. Amer. Meteor. Soc.*, **102**, E990–E1015, https://doi.org/10.1175/bams-d-19-0304.1.

Hui, W., W. Zhang, W. Lyu, and P. Li, 2020: Preliminary observations from the China Fengyun-4A lightning mapping imager and its optical radiation characteristics. *Remote Sens.*, **12**, 2622, https://doi.org/10.3390/rs12162622.

Joo, S., J. Eyre, and R. Marriott, 2013: The impact of MetOp and other satellite data within the Met Office global NWP system using an adjoint-based sensitivity method. *Mon. Wea. Rev.*, **141**, 3331–3342, https://doi.org/10.1175/MWR-D-12-00232.1.

Li, J., J. Li, J. Otkin, T. J. Schmit, and C. Liu, 2011: Warning information in a preconvection environment from the geostationary advanced infrared sounding system—A simulation study using IHOP case. *J. Appl. Meteor. Climatol.*, **50**, 776–783, https://doi.org/10.1175/2010JAMC2441.1.

Ma, L., D. Qin, L. Bian, C. Xiao, and Y. Luo, 2011: Assessment of snow cover vulnerability over the Qinghai-Tibetan Plateau. *Adv. Climate Change Res.*, **2**, 93–100, https://doi.org/10.3724/SP.J.1248.2011.00093.

Ma, Z., and Coauthors, 2021a: Four-dimensional wind fields from geostationary hyperspectral infrared sounder radiance measurements with high temporal resolution. *Geophys. Res. Lett.*, **48**, e2021GL093794, https://doi.org/10.1029/2021GL093794.

——, Z. Li, J. Li, T. J. Schmit, L. Cucurull, R. Atlas, and B. Sun, 2021b: Enhanced low level temperature and moisture profiles through combining NUCAPS, ABI observations and RTMA analysis. *Earth Space Sci.*, **8**, e2020EA001402, https://doi.org/10.1029/2020EA001402.

Menzel, W. P., T. J. Schmit, P. Zhang, and J. Li, 2018: Satellite-based Atmospheric Infrared Sounder development and applications. *Bull. Amer. Meteor. Soc.*, **99**, 583–603, https://doi.org/10.1175/BAMS-D-16-0293.1.

Miller, P. A., M. F. Barth, L. A. Benjamin, R. S. Artz, and W. R. Pendergrass, 2005: The Meteorological Assimilation and Data Ingest System (MADIS): Providing value-added observations to the meteorological community. *21st Conf. on Weather Analysis and Forecasting/17th Conf. on Numerical Weather Prediction*, Washington, DC, Amer. Meteor. Soc., P1.95, http://ams.confex.com/ams/WAFNWP34BC/techprogram/paper_98637.htm.

Min, M., and Coauthors, 2017: Developing the science product algorithm testbed for Chinese next-generation geostationary meteorological satellites: Fengyun-4 series. *J. Meteor. Res.*, **31**, 708–719, https://doi.org/10.1007/s13351-017-6161-z.

Schmetz, J., and W. P. Menzel, 2015: A look at the evolution of meteorological satellites: Advancing capabilities and meeting user requirements. *Wea. Climate Soc.*, **7**, 309–320, https://doi.org/10.1175/WCAS-D-15-0017.1.

Schmit, T. J., J. Li, S. A. Ackerman, and J. J. Gurka, 2009: High spectral and high temporal resolution infrared measurements from geostationary orbit. *J. Atmos. Oceanic Technol.*, **26**, 2273–2292, https://doi.org/10.1175/2009JTECHA1248.1.

Smith, W. L., 1991: Atmospheric soundings from satellites—False expectation or the key to improved weather prediction? *Quart. J. Roy. Meteor. Soc.*, **117**, 267–297, https://doi.org/10.1002/qj.49711749802..

——, H. E. Revercomb, H. B. Howell, H. M. Woolf, and D. D. LaPorte, 1987: The High Resolution Interferometer Sounder (HIS). *Atmospheric Radiation*, K. N. Liou and Z. Xiuji, Eds., Amer. Meteor. Soc., 271–281, https://doi.org/10.1007/978-1-935704-18-8_42.

——, and Coauthors, 2009: Evolution, current capabilities, and future advances in satellite nadir viewing ultra-spectral IR sounding of the lower atmosphere. *Atmos. Chem. Phys.*, **9**, 5563–5574, https://doi.org/10.5194/acp-9-5563-2009.

——, H. E. Revercomb, E. Weisz, D. C. Tobin, R. O. Knuteson, J. Taylor, and W. P. Menzel, 2021: Hyperspectral satellite radiance atmospheric profile information content and its dependence on spectrometer technology. *IEEE J. Sel. Top. Appl. Earth Obs. Remote Sens.*, **14**, 4720–4736, https://doi.org/10.1109/JSTARS.2021.3073482.

Weisz, E., N. Smith, and W. L. Smith, 2015: The use of hyperspectral sounding information to monitor atmospheric tendencies leading to severe local storms. *Earth Space Sci.*, **2**, 369–377, https://doi.org/10.1002/2015EA000122.

WMO, 1996: Guide to meteorological instruments and methods of observation. 6th ed. WMO Rep. 8, 501 pp.

Wulfmeyer, V., and Coauthors, 2015: A review of the remote sensing of lower tropospheric thermodynamic profiles and its indispensable role for the understanding and the simulation of water and energy cycles. *Rev. Geophys.*, **53**, 819–895, https://doi.org/10.1002/2014RG000476.

Yang, J., Z. Zhang, C. Wei, F. Lu, and Q. Guo, 2017: Introducing the new generation of Chinese geostationary weather satellites, Fengyun-4. *Bull. Amer. Meteor. Soc.*, **98**, 1637–1658, https://doi.org/10.1175/BAMS-D-16-0065.1.